Picosecond Acoustics in Single Quantum Wells of Cubic GaN/(Al,Ga)N

T. Czerniuk,[1,*] T. Ehrlich,[1] T. Wecker,[2] D. J. As,[2] D. R. Yakovlev,[1,3] A. V. Akimov,[4] and M. Bayer[1,3]

[1]*Experimentelle Physik 2, Technische Universität Dortmund, 44221 Dortmund, Germany*
[2]*Department of Physics, University of Paderborn, 33098 Paderborn, Germany*
[3]*Ioffe Physical-Technical Institute, Russian Academy of Sciences, 194021 St. Petersburg, Russia*
[4]*School of Physics and Astronomy, University of Nottingham, Nottingham NG7 2RD, United Kingdom*

A picosecond acoustic pulse is used to study the photoelastic interaction in single zinc-blende GaN/Al_xGa_{1-x}N quantum wells. We use an optical time-resolved pump-probe setup and demonstrate that tuning the photon energy to the quantum well's lowest electron-hole transition makes the experiment sensitive to the quantum well only. Because of the small width, its temporal and spatial resolution allows us to track the few-picosecond-long transit of the acoustic pulse. We further deploy a model to analyze the unknown photoelastic coupling strength of the quantum well for different photon energies and find good agreement with the experiments.

I. INTRODUCTION

During the last decade, picosecond acoustics have shown the ability for characterizing various nanostructures with nanometer and picosecond spatial and temporal resolution, respectively [1]. There are different methods to optically detect subterahertz and terahertz (THz) elastic waves (i.e., coherent phonons) with picosecond temporal resolution. They can be observed at the surface of bulk materials by optical transitions covering a broad spectral range from the ultraviolet (UV) to the near infrared [2]. If also in-depth information is required, an established technique is based on exploiting buried semiconductor quantum wells (QWs) [3–5]. Nitride semiconductor QWs [e.g., GaN/(InGa)N] are highly efficient nanostructures for the generation and detection of coherent phonons with frequencies of up to 2 THz [6]. Most of the experiments with nitride quantum wells are performed on multiple QWs based on wurtzite (hexagonal) h-GaN and its alloys. The piezoelectric effect in h-GaN is shown to be the most important mechanism for the generation and detection of coherent phonons. Experiments with zinc-blende (cubic) c-GaN, which does not possess piezoelectricity along the high-symmetry directions (e.g. [100]), were performed only on bulk layers [7,8]. The importance of c-GaN QWs in picosecond acoustics is related to the possibility of embedding c-GaN QWs into Si- or GaAs-based phononic chips, thus, allowing us to perform phononic engineering for nanoscopy [9] and electrophononic devices [10].

In the present paper, we report on picosecond acoustics experiments with c-GaN/Al_xGa_{1-x}N single QWs. We show that for a high x and an appropriate optical probing wavelength, the QW serves as a detector for subterahertz coherent phonons. The results show that the fabricated structures possess a sufficient quality for coherent phonon experiments and may be operated with UV optical pulses.

II. SAMPLE AND EXPERIMENT

A scheme of the sample is shown in Fig. 1(a). It is grown by molecular-beam epitaxy on a Si(100) substrate, which is polished to a thickness of 90 μm, followed by a 10-μm-thick buffer layer of 3C-SiC. On top, the actual sample structure is grown, consisting of a 100-nm c-GaN bulk layer and two 50-nm c-Al_xGa_{1-x}N barriers sandwiching the 10-nm-thick c-GaN single QW [11]. Two samples with an Al content of $x = 0.1$ and $x = 0.8$ are investigated. Photoluminescence spectra are recorded at $T = 15$ K and are shown for the QW with high barriers ($x = 0.8$, dashed curve) and a reference bulk layer (solid curve) in the bottom panel of Fig. 1(a). The bulk layer emits at a wavelength of about 380 nm, while the emission of the quantum well is observed slightly blueshifted at 375 nm. This difference corresponds to a quantization energy of $E_Q = 45$ meV. On the backside of the polished Si substrate, a 100-nm thin aluminum film is deposited, which is used to create a picosecond acoustic pulse, which we detail hereafter.

In our time-resolved pump-probe setup, we use two laser pulses originating from the same laser to create the acoustic pulse with the pump beam and to measure the induced changes of the optical properties with the probe beam. The light source is an optical parametric amplifier that provides pulses with a duration of 100 fs, a wavelength of 700–900 nm, and a repetition rate of 30 kHz. A beam splitter is used to split its output pulses. The pump beam is guided over a mechanical delay stage and focused on the backside of the sample to a spot with a diameter of about 100 μm. Here, the aluminum film absorbs the optical energy and subsequently heats up, leading to a rapid thermal
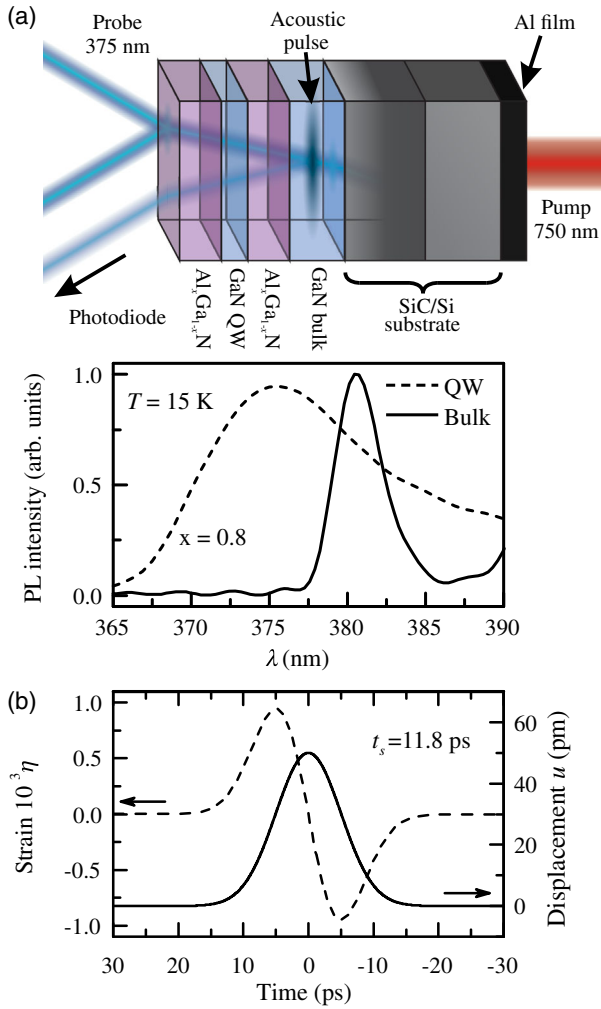
*thomas.czerniuk@tu-dortmund.de

FIG. 1. (a) Sketch of the sample (top) and photoluminescence spectra (bottom). The emission is recorded at $T = 15$ K from the QW with $x = 0.8$ (dashed) and a c-GaN bulk layer (solid). (b) Temporal displacement $u(t)$ and strain $\eta(t)$ profiles of the acoustic pulse, which is generated in the Al film on the backside of the sample.

expansion. As a result, an acoustic pulse is launched into the Si substrate, which propagates towards the c-GaN QW on the sample's front side with the sound velocity v [12]. To prevent a strong attenuation of the acoustic pulse during the Si/SiC substrate transit, the sample is placed into a flow cryostat and cooled down to 40 K [13]. The input acoustic pulse is depicted in Fig. 1(b), where the displacement $u(t)$ and its derivative with respect to the propagation direction, the strain $\eta(t)$, are shown. The displacement can be modeled by a Gaussian with a duration determined by the optical absorption length μ_{Al} and sound velocity v_{Al} and its FWHM is found to be $\tau_S = \mu_{Al}/v_{Al} = 12$ ps [14]. For the applied optical excitation energies, the amplitude is in the order of 50 pm, which corresponds to a maximum strain of about 10^{-4}–10^{-3}.

The acoustic pulse is detected by the probe beam when it passes the GaN bulk and QW layers. For the best efficiency,

the probe beam needs to be frequency doubled to make the photon energy match the electronic transitions in these regions. It is incident on the front surface under an angle of about $\theta_1 = 40°$ and focused to a spot of about 30 μm diameter. We measure the reflection $S(t)$ with a photodiode and increase the sensitivity by using a lock-in detector and a mechanical chopper, which is placed in the pump beam pathway. In this configuration, the dominant term in the signal is the interference of the part of the probe beam, which is reflected at the surface, with the reflection originating from the acoustic pulse.

III. RESULTS AND DISCUSSION

At first we present the results obtained from the sample with the low Al content in the barriers, $x = 0.1$. The temporal signals $S(t)$ recorded for a pump excitation density $W = W_0 \sim 1$ mJ/cm^2 are shown in Fig. 2(a) for three probe wavelengths λ. Their fast Fourier transforms (FFTs) presented in Fig. 2(b) show a spectral line, whose maximum f_B (marked by the vertical arrows) increases slightly with the decrease of the wavelength λ from $f_B = 112$ GHz at $\lambda = 380$ nm to $f_B = 118$ GHz at $\lambda = 370$ nm. This spectral line is attributed to the so-called Brillouin oscillations, which appear in thick films due to the dynamic interference between the part of the probe beam being reflected from the picosecond strain pulse and from the surface of the sample [15]. One easily finds that

$$f_B = \frac{2v}{\lambda}\sqrt{n^2 - \sin^2(\theta_1)}, \quad (1)$$

where n is the refractive index. Using the low-temperature value for the sound velocity in c-GaN $v_{GaN} = 6950$ m/s, $n = 2.7$ for the used λ, and $\theta_1 = 40°$, we obtain $f_B = 99$ GHz at $\lambda = 380$ nm and $f_B = 103$ GHz at $\lambda = 365$ nm. This 13% difference could be due to the altered values for n
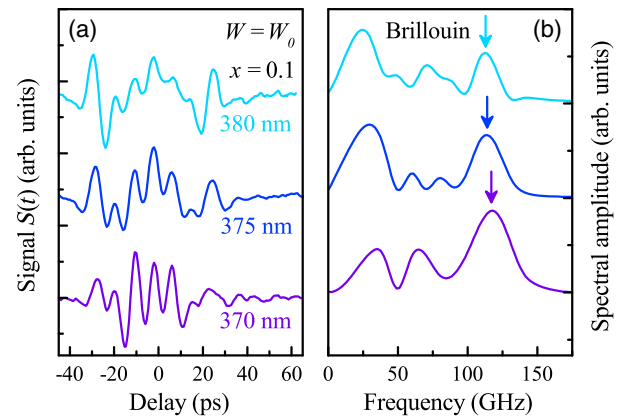

FIG. 2. (a) Measured signals $S(t)$ in the sample with $x = 0.1$ for three probe wavelengths λ. The curves are shifted vertically for clarity. (b) Fast Fourier transforms of the traces in (a). The peaks associated with Brillouin oscillations are marked by arrows.

and v in the GaN/(AlGa)N heterostructures compared to bulk GaN. However, the signals presented on Fig. 2(a) do not show any typical features related to the existence of the c-GaN QW in the sample. This is not surprising because for $x = 0.1$ the elastic and optical properties of the $Al_xGa_{1-x}N$ barriers and the GaN layers are quite similar, so the sample can be considered as a monolithic block with material parameters close to GaN. The detailed analysis of the measured $S(t)$ does not concern the QW and will not be considered further.

Now we turn to the results obtained on the sample with an Al content of $x = 0.8$. These are presented as solid lines in Fig. 3 for three probe wavelengths and for a pump excitation density of W_0 and $4W_0$ in Figs. 3(a) and 3(b). The signals $S(t)$ are very different from the case of $x = 0.1$: the Brillouin oscillations are strongly suppressed, and the corresponding spectral peaks at f_B in the FFTs of $S(t)$ (not shown) cannot be identified. For the shortest probe wavelength of $\lambda = 370$ nm [see the lowest curves in Figs. 3(a) and 3(b)], $S(t)$ has a simple shape, which is typical for a picosecond strain pulse detected in a thin layer near the surface [3,4]. We attribute this signal to the response of the c-GaN QW to the picosecond strain pulse. The extension of the photoexcited carrier wave functions in the high-quality QW with $d_{QW} = 10$ nm governs the temporal resolution limit of $d_{QW}/v_{GaN} \approx 1.4$ ps, which is short enough to resolve the main temporal features of the strain pulse. The shape of $S(t)$ is symmetric, and its total
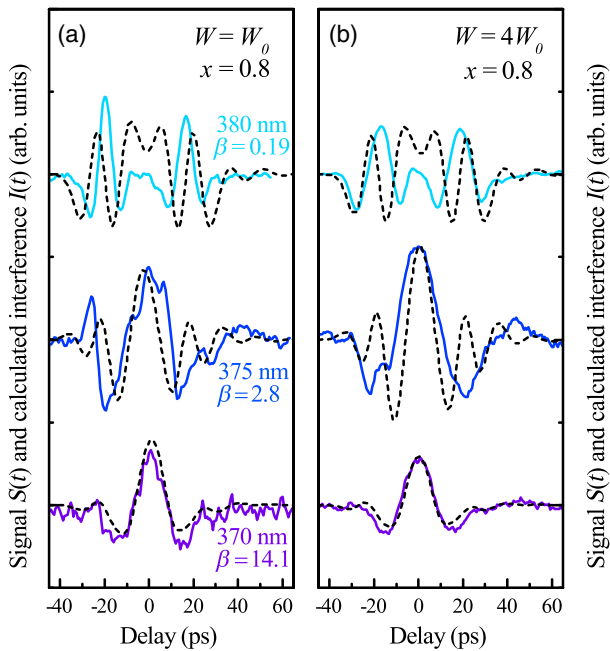

FIG. 3. (a) Measured signal $S(t)$ in the sample with $x = 0.8$ for a pump power of W_0 and three different probe wavelengths. The curves are shifted vertically for clarity. Calculations $I(t)$ with the corresponding value for β are presented as dashed lines. (b) Same as (a) but for a higher pump power of $4W_0$.

duration is $\tau_R \approx 40$ ps for the two studied pump excitation densities W. For longer probe wavelengths, the shape of $S(t)$ becomes more complicated [see the upper and middle curves in Figs. 3(a) and 3(b)]. The modulation of reflectivity starts earlier and finishes later relative to the case of $\lambda = 370$ nm. This means that with the increase of λ, the probe signal becomes more sensitive to the layers where the strain pulse appears earlier and leaves later, which are the ones located further from the sample surface. This observation cannot be explained by the longer penetration depth of probe light with the increase of λ, since the $Al_{0.8}Ga_{0.2}N$ barriers are transparent for light with $\lambda > 300$ nm [16], and only a small fraction of the probe light is absorbed by the 10-nm-thick QW [17]. On a qualitative level, it is clear that such an experimental behavior occurs if the relative contribution to the signal at $\lambda = 370$ nm is mostly due to the QW, and at $\lambda = 380$ nm the contribution for the bulk c-GaN layer is essential. This explanation is in agreement with the assumption that the $Al_{0.8}Ga_{0.2}N$ barriers do not give a contribution to the signal at any wavelength. Below, we show that the λ dependence of the measured reflectivity change is explained by different λ dependences of the photoelastic constants in the c-GaN/$Al_{0.8}Ga_{0.2}N$ QW and the bulk c-GaN layer.

To understand the strong λ dependence of $S(t)$, we discuss the two main contributions by which the acoustic pulse interacts with the probe light. The first one is the photoelastic effect: applying strain to a semiconductor modulates its band gap, thereby changing its refractive index $\tilde{n}$ (both the real part n and the imaginary part κ):

$$\Delta\tilde{n}(E) = \left(\frac{\partial n(E)}{\partial E} + i\frac{\partial\kappa(E)}{\partial E}\right)\frac{\partial E}{\partial\eta}\Delta\eta. \qquad (2)$$

The magnitude of the photoelastic coupling is proportional to the deformation potential that links the strain with the band-gap shift ($\partial E/\partial\eta \approx -7$ eV [18]) and to the dispersion slope of n and κ [19]. It is advantageous to operate near the band gap, where the dispersions are particularly steep. The second contribution is related to the interference of the reflected light from the surface and the interfaces inside the sample: when the acoustic pulse passes such an interface, it is moved. This displacement directly translates into a phase shift of the reflection originating from this interface with respect to all the other reflections, and, consequently, the acoustic pulse can be observed by the interference terms.

Both contributions are, in general, of similar magnitude and possess a λ dependence. However, although the strong difference of $S(t)$ for 370 and 380 nm indicates that the photoelastic effect is probably the dominant contribution, a detailed analysis is performed to exclude that the interface mechanism is responsible for the found behavior. In the beginning, we restrict our simulations to the photoelastic effect in the 100-nm GaN bulklike layer and the interface

mechanism, since the complex index of refraction dispersion is known only for bulk material [20] but not for the QW. A model to calculate the reflectivity change ΔR normalized to the unperturbed value R_0, which covers both effects, was developed before and is applied here to our experiment [12,21].

We use an input acoustic pulse like that shown in Fig. 1(b) and calculate its propagation through the heterostructure with the transfer-matrix and scattering-states methods to obtain the strain and displacement profiles $\eta(z, t)$ and $u(z, t)$, respectively. These profiles include all reflections at the layer interfaces and at the sample's surface [22,23]. For the simulations, we use a sound velocity of 6950 m/s for GaN [7] and 10 300 m/s for pure AlN, which is deduced from the calculated elastic constants in Ref. [24]. The sound velocity in the $Al_xGaN_{1-x}N$ alloy is assumed to be the mean of AlN and GaN weighted by x. For all studied wavelengths, the interface displacement contribution and the photoelastic contribution (neglecting the QW so far) to $\Delta R/R_0$ are separately calculated and presented in Fig. 4 as dashed and solid lines, respectively. Here, the delay $t = 0$ ps corresponds to the time at which the center of the acoustic pulse reaches the sample's surface.

The simulations show that the photoelastic response exceeds the interface displacement effect in all cases. This is most notably the case at a probe wavelength of $\lambda = 370$ nm, where the latter contribution is especially small because it is approaching the wavelength of 368 nm (not shown) where it flips its sign. For increasing wavelength, the interface displacement effect becomes stronger, but its overall shape does not change significantly. The photoelastic contribution is also most pronounced for 380 nm, close to the absorption edge of GaN [cf. Fig. 1(a)]. Here, the steep rise of absorption leads to a high slope of the imaginary part of $\tilde{n}$ that is responsible for the high photoelastic efficiency. Since the real part of the refractive index possesses a maximum at this wavelength, its slope is

small right at the resonance. For $\lambda = 370$ nm, there are two statements which may be made from the analysis and the comparison with the experimental results in Fig. 3: (i) the photoelastic contribution strongly dominates in the calculated curve, and (ii) the simulation does not resemble the measured signal [cf. the lowest line in Fig. 3]. This leads us to the main conclusion of our work that the signal measured for $\lambda = 370$ nm should have a significant contribution from the photoelastic effect in the QW.

Without detailed knowledge of the optical properties of the QW close to the electronic resonances, we take the bulk dispersion of $\tilde{n}$ and shift it by the quantization energy of the QW, which is about $E_Q = 45$ meV [cf. Fig. 1(a)]. In this simplified assumption of our analysis, we obviously neglect the differences between the bulk and QW dispersion arising from the additional electronic transitions in the QW. These transitions need to be considered when calculating the dielectric function correctly via the Kramers-Kronig relation [25]. However, this procedure is a large-scale effort, and we, therefore, use for simplicity a parameter α by which we multiply the shifted dispersion to obtain values for the QW that can reproduce our experimental findings:

$$\Delta\tilde{n}_{QW}(E) = \alpha\frac{\partial\tilde{n}(E - E_Q)}{\partial E}\frac{\partial E}{\partial\eta}\Delta\eta. \qquad (3)$$

Note that α also accounts for deviations from the bulk deformation potential that are, however, in the order of the quantization energy and, therefore, negligible. When α is found, we finally compare the ratio β of the photoelastic coupling efficiency of the QW with the one of the bulk layer. For this purpose, we divide the found absolute of $\Delta\tilde{n}_{QW}$ by the one of the bulk layer for each studied wavelength:

$$\beta(E) = \frac{\alpha|\partial\tilde{n}(E - E_Q)/\partial E|}{|\partial\tilde{n}(E)/\partial E|}. \qquad (4)$$

The simulated signals comprising the photoelastic effect in bulk and QW and the interface displacement are presented as dashed lines in Figs. 3(a) and 3(b). In the case of $\lambda = 370$ nm, the probe wavelength falls into the high-energy flank of the QW resonance, and the simulations require a large scaling factor of $\alpha = 3.5$ for good agreement. This is quite reasonable: the shifted bulk dispersion we assume for the QW lacks the additional higher electronic transitions supported by the QW, which have a significant contribution to the refractive index (especially to the extinction coefficient κ). Therefore, a larger refinement of the model is necessary for probe wavelengths interacting with these neglected transitions, which are wavelengths shorter than 375 nm for the QW studied here. The calculated curves resemble well the main features of the experiment, i.e., the central peak and the neighboring dips. First, a decrease of $S(t)$ is observed when
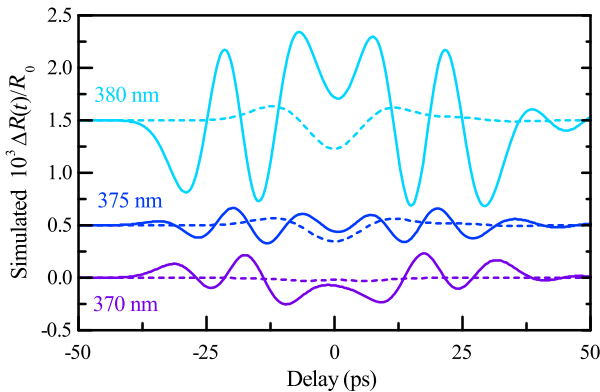

FIG. 4.   Simulation for the relative reflectivity change $\Delta R/R_0$ due to the photoelastic effect in the GaN bulk layer (solid lines) and the interface displacement (dashed lines) for the three studied wavelengths λ. The curves are shifted vertically for clarity.

the leading negative part of the strain pulse [cf. Fig. 1(b)] passes the QW, while the following part of tensile strain consequently leads to an increase. At the sample surface, the strain pulse is reflected and flips its sign. Since the QW is only 50 nm away from the sample surface, the tensile parts of the incident and of the reflected strain pulse superpose constructively at the QW and lead to the dominant positive peak at $t = 0$ ps. The simulation reveals that the photoelastic coupling efficiency in the QW is about $\beta = 14.1$ times stronger than that of the bulk layer, mainly due to the steep slope of the extinction coefficient κ.

For a higher probe wavelength of $\lambda = 375$ nm, the contribution from the bulk layer becomes apparent, as we observe a peak at earlier times $t = -26$ ps. In the simulations, we leave $\alpha = 1$ for good agreement, which yields several additional peaks originating from the bulk layer that can also be seen in the experimental signal. We obtain $\beta = 2.8$ and conclude that the strain pulse is mainly detected by the QW. The photoelastic coefficient of the bulk layer is relatively small because the bulk layer is still transparent for this wavelength [cf. Fig. 1(a)].

The shape of the signal changes significantly only when the probe wavelength is increased further to $\lambda = 380$ nm, as shown in the upper curves in Figs. 3(a) and 3(b). There is no peak at $t = 0$, but instead there are two symmetric features at $t = \pm 18$ ps. Good agreement with the experiment is achieved for $\alpha = 0.7$, which corresponds to $\beta = 0.19$. The signal is governed by the contribution from the bulk layer, since it is almost resonant here. Its contribution clearly dominates the signal, and the simulated curve looks similar to the one in which the QW is not included at all.

Even for the parameter α giving the best results, some discrepancies between the experiments and simulations (solid and dashed lines in Fig. 3, respectively) remain: most remarkably, the different duration of the signal, e.g., for $\lambda = 375$ nm and the nonvanishing central peak at $t = 0$ for $\lambda = 380$ nm. Also, if n and κ are scaled independently, the experiment cannot be better reproduced. We explain the remaining discrepancies by the unknown precise extension of the electron and hole wave functions. Moreover, the sound velocity in thin and strained cubic GaN/Al$_x$Ga$_{1-x}$N films might be different than assumed. We have also not considered a nonlinear acoustic pulse propagation through the Si/SiC substrate: for high strain amplitudes, lattice anharmonicity and dispersive effects lead to sharp flanks and increase the total duration of the pulse [26]. Taking into account nonlinear propagation might explain the missing sharp features for $\lambda = 375$ nm and the slightly broader peaks for $\lambda = 380$ nm at the higher excitation energy of $4W_0$ [cf. Fig. 3(b)] compared to the respective signals measured for W_0.

IV. CONCLUSION

In conclusion, we show experimentally that a high-quality single QW of c-GaN is capable of detecting picosecond strain waves. The temporal and spatial resolution limit of 1.4 ps and 10 nm is determined by the speed of sound and the QW thickness. By tuning the probe wavelength to the QW resonance, the signal can be well separated from adjacent bulk layers of the same material, making c-GaN QWs attractive candidates for ultrafast strain detectors in zinc-blende materials.

The presented results open the prospective application of using ultrafast acoustics in UV optoelectronics and nano-photonics. Picosecond strain pulses in GaN QWs may be used for the modulation of UV light sources. The amplitude modulation of the laser emission in this case may reach 100%, similar to experiments performed in the near infra-red with GaAs-based vertical lasers [27,28]. Another attractive field for application is UV nanoscopy [9], where the combination of short optical wavelengths and pico-second strain pulses allows one to reach nanometer resolution in measuring photonic and plasmonic fields and defects buried in GaN-based nanostructures.

[1] O. Matsuda, M. C. Larciprete, R. L. Voti, and O. B. Wright, Fundamentals of picosecond laser ultrasonics, Ultrasonics **56**, 3 (2015).

[2] P. Babilotte, P. Ruello, D. Mounier, T. Pezeril, G. Vaudel, M. Edely, J.-M. Breteau, V. Gusev, and K. Blary, Femtosecond laser generation and detection of high-frequency acoustic phonons in GaAs semiconductors, Phys. Rev. B **81**, 245207 (2010).

[3] O. Matsuda, T. Tachizaki, T. Fukui, J. J. Baumberg, and O. B. Wright, Acoustic phonon generation and detection in GaAs/Al$_{0.3}$Ga$_{0.7}$As quantum wells with picosecond laser pulses, Phys. Rev. B **71**, 115330 (2005).

[4] A. V. Akimov, A. V. Scherbakov, D. R. Yakovlev, C. T. Foxon, and M. Bayer, Ultrafast Band-Gap Shift Induced by a Strain Pulse in Semiconductor Heterostructures, Phys. Rev. Lett. **97**, 037401 (2006).

[5] D. Moss, A. V. Akimov, R. P. Campion, M. Henini, C. T. Foxon, L. Eaves, A. J. Kent, and B. A. Glavin, Picosecond strain pulses probed by the photocurrent in semiconductor devices with quantum wells, Phys. Rev. B **83**, 245303 (2011).

[6] C.-K. Sun, J.-C. Liang, and X.-Y. Yu, Coherent Acoustic Phonon Oscillations in Semiconductor Multiple Quantum Wells with Piezoelectric Fields, Phys. Rev. Lett. **84**, 179 (2000).

[7] D. Moss, A. V. Akimov, S. V. Novikov, R. P. Campion, C. R. Staddon, N. Zainal, C. T. Foxon, and A. J. Kent, Elasto-optical properties of zinc-blende (cubic) GaN measured by picosecond acoustics, J. Phys. D **42**, 115412 (2009).

[8] Chuan He, Martin Grossmann, Delia Brick, Martin Schubert, Sergei V. Novikov, C. Thomas Foxon, Vitalyi Gusev, Anthony J. Kent, and Thomas Dekorsy, Study of confined coherent acoustic phonon modes in a free-standing cubic GaN membrane by femtosecond spectroscopy, Appl. Phys. Lett. **107,** 112105 (2015).

[9] K.-H. Lin, C.-M. Lai, C.-C. Pan, J.-I. Chyi, J.-W. Shi, S.-Z. Sun, C.-F. Chang, and C.-K. Sun, Spatial manipulation of nanoacoustic waves with nanoscale spot sizes, Nat. Nanotechnol. **2,** 704 (2007).

[10] D. M. Moss, A. V. Akimov, B. A. Glavin, M. Henini, and A. J. Kent, Ultrafast Strain-Induced Current in a GaAs Schottky Diode, Phys. Rev. Lett. **106,** 066602 (2011).

[11] J. Schörmann, S. Potthast, D. J. As, and K. Lischka, *In situ* growth regime characterization of cubic GaN using reflection high energy electron diffraction, Appl. Phys. Lett. **90,** 041918 (2007).

[12] C. Thomsen, H. T. Grahn, H. J. Maris, and J. Tauc, Surface generation and detection of phonons by picosecond light pulses, Phys. Rev. B **34,** 4129 (1986).

[13] B. C. Daly, K. Kang, Y. Wang, and D. G. Cahill, Picosecond ultrasonic measurements of attenuation of longitudinal acoustic phonons in silicon, Phys. Rev. B **80,** 174112 (2009).

[14] A. D. Rakić, A. B. Djurišić, J. M. Elazar, and M. L. Majewski, Optical properties of metallic films for vertical-cavity optoelectronic devices, Appl. Opt. **37,** 5271 (1998).

[15] C. Thomsen, H. T. Grahn, H. J. Maris, and J. Tauc, Picosecond interferometric technique for study of phonons in the Brillouin frequency range, Opt. Commun. **60,** 55 (1986).

[16] F. Yun, M. A. Reshchikov, L. He, T. King, H. Morko, S. W. Novak, and L. Wei, Energy band bowing parameter in $Al_xGa_{1-x}N$ alloys, J. Appl. Phys. **92,** 4837 (2002).

[17] D. Brunner, H. Angerer, E. Bustarret, F. Freudenberg, R. Höpler, R. Dimitrov, O. Ambacher, and M. Stutzmann, Optical constants of epitaxial AlGaN films and their temperature dependence, J. Appl. Phys. **82,** 5090 (1997).

[18] R. Riane, A. Zaoui, S. F. Matar, and A. Abdiche, Pressure dependence of electronic and optical properties of zinc-blende GaN, BN and their $B_{0.25}Ga_{0.75}N$ alloy, Physica (Amsterdam) **405B,** 985 (2010).

[19] A. Bartels, T. Dekorsy, H. Kurz, and K. Köhler, Coherent Zone-Folded Longitudinal Acoustic Phonons in Semiconductor Superlattices: Excitation and Detection, Phys. Rev. Lett. **82,** 1044 (1999).

[20] M. Feneberg, M. Röppischer, C. Cobet, N. Esser, J. Schörmann, T. Schupp, D. J. As, F. Hörich, J. Bläsing, A. Krost, and R. Goldhahn, Optical properties of cubic GaN from 1 to 20 eV, Phys. Rev. B **85,** 155207 (2012).

[21] O. Matsuda, O. B. Wright, D. H. Hurley, V. Gusev, and K. Shimizu, Coherent shear phonon generation and detection with picosecond laser acoustics, Phys. Rev. B **77,** 224110 (2008).

[22] S. Tamura, D. C. Hurley, and J. P. Wolfe, Acoustic-phonon propagation in superlattices, Phys. Rev. B **38,** 1427 (1988).

[23] A. V. Kavokin, G. Malpuech, A. Di Carlo, M. Vladimirova, P. Lugli, and F. Rossi, Optical polarization grating in semiconductors induced by exciton polaritons, Phys. Rev. B **60,** 15554 (1999).

[24] A. F. Wright, Elastic properties of zinc-blende and wurtzite AlN, GaN, and InN, J. Appl. Phys. **82,** 2833 (1997).

[25] Mandy M. Y. Leung, Aleksandra B. Djurii, and E. Herbert Li, Refractive index of InGaN/GaN quantum well, J. Appl. Phys. **84,** 6312 (1998).

[26] H.-Y. Hao and H. J. Maris, Experiments with acoustic solitons in crystalline solids, Phys. Rev. B **64,** 064302 (2001).

[27] C. Brüggemann, A. V. Akimov, A. V. Scherbakov, M. Bombeck, C. Schneider, S. Höfling, A. Forchel, D. R. Yakovlev, and M. Bayer, Laser mode feeding by shaking quantum dots in a planar microcavity, Nat. Photonics **6,** 30 (2012).

[28] T. Czerniuk, C. Brüggemann, J. Tepper, C. Schneider, M. Kamp, S. Höefling, B. A. Glavin, D. R. Yakovlev, A. V. Akimov, and M. Bayer, Lasing from active optomechanical resonators, Nat. Commun. **5,** 4038 (2014).